

Supplementary Information

Relating Mechanical Properties and Chemical Bonding in an Inorganic-Organic Framework Material: A Single-Crystal Nanoindentation Study

Jin Chong Tan,[†] Joshua D. Furman,[‡] and Anthony K. Cheetham^{*†}

Department of Materials Science and Metallurgy, University of Cambridge, Pembroke Street, Cambridge CB2 3QZ, U.K., and Materials Research Laboratory, University of California, Santa Barbara, California 93106.

Table of Contents

1	Experimental Procedures	S2
1.1	Synthesis of Ce(C ₂ O ₄)(HCO ₂)	S2
1.2	Single-Crystal X-Ray Diffraction	S2
1.3	Nanoindentation Experiments	S2
1.4	Atomic Force Microscopy (AFM)	S4
2	Analysis of Nanoindentation Data	S4
2.1	Young's Modulus (<i>E</i>)	S4
2.2	Hardness (<i>H</i>)	S5
2.3	Indentation Work	S5
2.4	Indentation Stress and Strain	S6
	References	S13

[†] University of Cambridge
[‡] University of California

1 Experimental Procedures

1.1 Synthesis of $\text{Ce}(\text{C}_2\text{O}_4)(\text{HCO}_2)$

$\text{Ce}(\text{C}_2\text{O}_4)(\text{HCO}_2)$, **1**, was prepared by hydrothermal synthesis. The synthesis was modified from that reported by Romero et al.,¹ to yield larger crystals. A mixture of 0.15 mmol $\text{Ce}(\text{OH})_4$ (Aldrich) and 1 mmol oxalic acid (Aldrich) in 10 mL deionized water was sealed in a 23 mL PTFE-lined Parr[®] autoclave. The autoclave was heated at 200 °C for 5 days. During heating, a portion of oxalic acid decomposed to formic acid and the cerium(IV) was reduced to cerium(III) by the acidic solution. The final product, consisting of colorless block crystals ($\sim 200 \times 50 \times 45 \mu\text{m}^3$) were recovered by filtration, washed with water and ethanol, and then dried in air.

1.2 Single-Crystal X-Ray Diffraction

Single-crystal X-ray diffraction was carried out to confirm the crystal structure of **1**, and to index the primary crystal facets (see Figure 1a in main text) for nanoindentation testing. A representative single-crystal was selected under the polarizing microscope and glued onto a glass fiber using epoxy. The crystal structure determination was performed on a Bruker single crystal diffractometer using a Nonius FR591 rotating anode source with a molybdenum target ($\lambda = 0.71073 \text{ \AA}$) and a KappaCCD detector with graphite monochromator. A hemisphere of intensity data were collected at 120 K. An empirical correction on the basis of symmetry equivalent reflections was applied using the SADABS program.² The structure was solved by direct methods using SHELXTL and difference Fourier syntheses.³ The hydrogen atoms were found in the Fourier difference map and constrained to chemically reasonable positions. Summary of the crystal structure data are listed in Table S1, and the full dataset can be found in the Crystallographic Information File (CIF).

1.3 Nanoindentation Experiments

Nanoindentation was performed at ambient temperature using an MTS NanoIndenter[®] XP (MTS Corp., Eden Prairie, MN), equipped with the Continuous Stiffness Measurement (CSM) module. The instrument was placed within an isolation cabinet that shielded against thermal instability and acoustic interference. Two types of diamond indenter tips were used: (i) A three-

sided pyramidal Berkovich indenter with a sharp tip (end radius ~ 100 nm) was used to determine the Young's modulus (E) and hardness (H). (ii) A spherical tipped indenter (nominal radius, $R=10$ μm) was employed to study the elastic-plastic transition and to characterize the strain-hardening characteristics in the plastic regime.

Calibration was performed using a fused silica standard, with elastic modulus ($E=72$ GPa) and hardness ($H=9$ GPa) that are of the same order of magnitude as the hybrid crystals being investigated here. Thermal drifts were ensured to be consistently low (typically < 0.05 nm s^{-1}). To avoid interaction of deformed zones, the inter-indent spacing was ensured to be at least 50 times the indentation depth (Figure S1).

Untwinned single crystals were used in our nanoindentation studies. The surfaces of as-synthesized crystals can be uneven due to growth steps and dissolution pits, with heights and/or depths ranging from tens of nanometers to several microns. Surface features with roughness amplitude larger than that of the contact dimension (end radius of sharp tip) can impair surface contact detection and result in inaccurate contact area determination. To overcome these, individual crystals were cold-mounted using the Epofix resin (Struers Ltd.) and then carefully polished using increasingly fine diamond suspensions, followed by a final polishing step using 0.05 μm colloidal silica suspension. The final (rms) surface roughness was found to be of less than 10 nm, as determined from AFM topographic images. The mounted and polished crystal surfaces were oriented to within $\sim 0.1^\circ$ of the desired orientation (i.e. normal to the indenter axis).

Nanoindentation experiments were conducted under the dynamic displacement-controlled CSM mode, so that E and H can be determined as a function of indentation depth (Figure S2). This was achieved by superimposing a 2 nm sinusoidal displacement at 45 Hz onto the primary loading signal, while tracking the system response via a frequency-specific amplifier.⁴ The loading and unloading strain rates were set at 5×10^{-2} s^{-1} . At the preset displacement of 500 nm, the indenter was held for 30 seconds prior to unloading in order to minimize creep effects.

1.4 Atomic Force Microscopy (AFM)

The shape of the residual indents was characterized using a Veeco Dimension V scanning probe microscope (SPM), under tapping-mode to map the 3-D morphology of the residual indents after complete unloading. All scans were carried out at a 512×512 resolution. The gain and proportional gain were set at 4 and 40, respectively. An amplitude setpoint of 310 mV was applied and the scan rate was set at 0.4 Hz.

2 Analysis of Nanoindentation Data

2.1 Young's Modulus (E)

By applying the dynamic CSM mode nanoindentation procedures described in Section 1.3, the Young's modulus (E) can be obtained as a function of surface penetration depth (h). This is achieved by continuously monitoring the change in the elastic contact stiffness (S), which was subsequently used to calculate the reduced modulus (E_r):⁵

$$E_r = \frac{\sqrt{\pi}}{2\beta} \frac{S}{\sqrt{A_c}} \quad (1)$$

where A_c is the contact area under load (predetermined from a calibrated tip areal function), and β is a constant that depends on the geometry of the indenter ($\beta=1.034$ for a Berkovich tip, and $\beta=1$ for a spherical tip).

The method of Oliver and Pharr⁶ was used to extract the sample elastic modulus (E) from the reduced modulus (E_r) given in eqn.(1).

$$\frac{1}{E_r} = \left(\frac{1-\nu_s^2}{E} \right) + \left(\frac{1-\nu_i^2}{E_i} \right) \quad (2)$$

where E_i and ν_i are the elastic modulus and Poisson's ratio of the indenter, respectively (for the diamond tip: $E_i = 1141$ GPa and $\nu_i = 0.07$). It is noted that the calculated value of E is not sensitive towards the choice of the sample Poisson's ratio (ν_s). For instance, ν_s of 0.2 ± 0.1 only results in an $\sim 5\%$ uncertainty in the final value of E . In the main text, all elastic moduli presented were calculated using $\nu_s = 0.2$.

2.2 Hardness (H)

The hardness, H , is determined by dividing the applied load (P) by the contact area developed under that load (A_c):

$$H = \frac{P}{A_c} \quad (3)$$

whereby A_c is calculated from the contact depth (h_c), which is modelled as the contact between a paraboloid of revolution with an elastic half-space, given by:⁶

$$h_c = h_{\max} - 0.75 \left(\frac{P}{S} \right) \quad (4)$$

where h_{\max} is the maximum indentation depth, and $0.75(P/S)$ denotes the extent of elastic recovery. Refer to Figure S2a for more details.

2.3 Indentation Work

The total work (W_{tot}) done during an indentation test consists of elastic work (W_{el}) and plastic work (W_{pl}), as depicted in Figure S3. By calculating the contribution of the elastic work (in percentage, $\left(\frac{W_{\text{el}}}{W_{\text{tot}}} \right) \times 100\%$), we can access the extent of elastic recovery when the indenter tip is being withdrawn from the maximum penetration depth.

The total work done by the indenter corresponds to the area lying under the loading curve (see Figure S3a), and can be determined by:

$$W_{\text{tot}} = \int_0^{h_{\max}} P(h) dh \quad (5)$$

During the unloading stage (see Figure S3b), the strain energy restored (as a result of elastic recovery) can be calculated by numerically integrating the area under the unloading curve:

$$W_{\text{el}} = \int_{h_f}^{h_{\max}} P(h) dh \quad (6)$$

Table S2 lists the percentages of elastic work for the (010)-, (100)- and (001)-oriented facets of compound **1**, as obtained via spherical-tipped nanoindentation.

2.4 Indentation Stress and Strain

Under a spherical-tipped indenter, the indentation stress (P_m) represents the mean contact pressure (i.e. hardness):⁷

$$P_m = \frac{P}{\pi a^2} \quad (7)$$

In this case, the relationship between contact radius (a) and contact depth (h_c) is given by $a = \sqrt{2Rh_c - h_c^2}$ if we assume there is no pile-up.⁸

In the elastic regime, P_m is linearly proportional to the indentation strain ($\varepsilon = a/R$), as given by the Hertzian relationship:⁹

$$P_m = \frac{4E_r}{3\pi} \left(\frac{a}{R} \right) \quad (8)$$

where R is the radius of the spherical tip and E_r is the reduced modulus (eqn.(1)). At lower strain levels ($a/R < \sim 0.1$), the crystal faces are deforming elastically since a linear Hertzian relationship defined by eqn.(8) can be used to relate stress and strain. The straight lines (see Figure 3 (inset) in the main text) indicate the expected stress-strain relationships for purely elastic loading. The yield pressure (P_y) denotes the critical stress corresponding to an elastic-plastic transition, i.e. when the stress-strain curve starts to deviate from linearity.

Table S1: Summary of the crystal structure data of cerium oxalate-formate.

Formula	Ce(C ₂ O ₄)(HCO ₂)
Molecular Weight	273.16
Crystal System	Orthorhombic
Space Group	<i>Pna</i> 2 ₁ (33)
a/Å	7.3280
b/Å	6.7430
c/Å	10.8160
Vol/Å ³	534.47
Z	4
Density/g cm ⁻³	3.395
2θ Range	8.22-54.92
Data/restrains/parameters	1113/1/46
R _{int}	0.0171
wR ₂ (I > 2σ(I))	0.0432
R (all data)	0.0174

Table S2: Elastic and plastic work measured along the three primary crystal facets of compound **1**, as obtained from a spherical-tipped nanoindenter ($h_{\max}=500$ nm). Refer to the schematics in Figure S3 for details on the areas considered for calculating W_{el} and W_{tot} .

Crystal Facet	Elastic work W_{el} (nJ)	Total work W_{tot} (nJ)	Percentage of Elastic Work $\left(\frac{W_{\text{el}}}{W_{\text{tot}}}\right) \times 100\%$
(010)	7.36	8.03	91.7
(100)	6.19	8.56	72.3
(001)	7.12	13.1	54.4

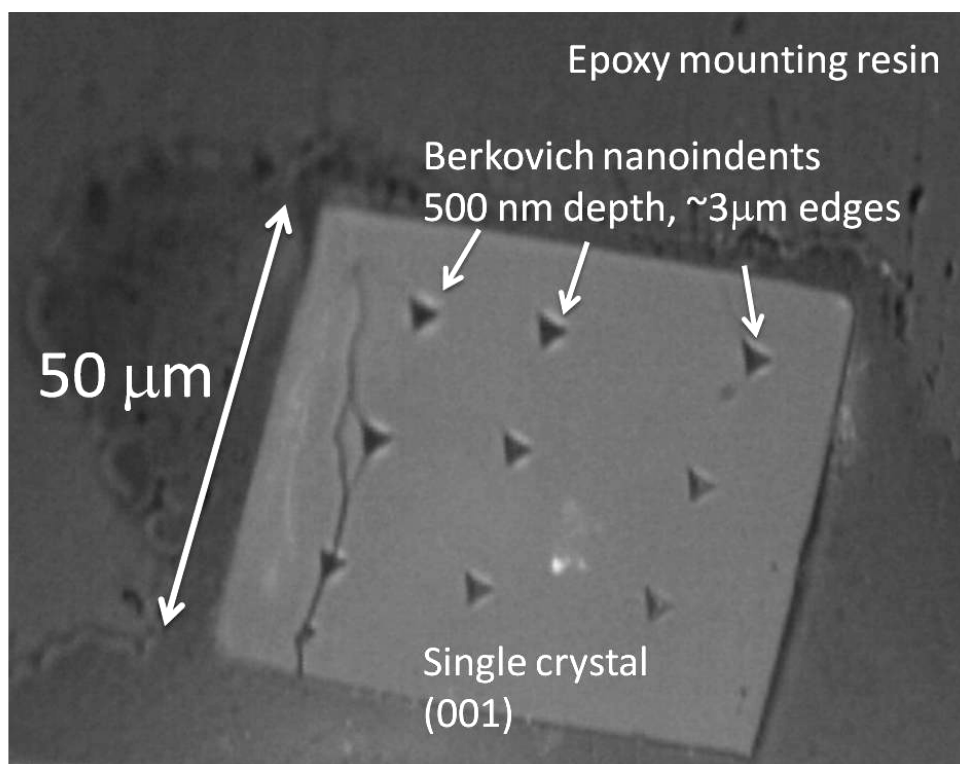


Figure S1: Optical micrograph of a single crystal of **1** with an exposed (001)-oriented facet. Shown here are the residuals of the Berkovich indents made in a (3×3) array, to a maximum depth, h_{max} of 500 nm. Note that indents that fell on an existing crack were discounted from the modulus and hardness analyses.

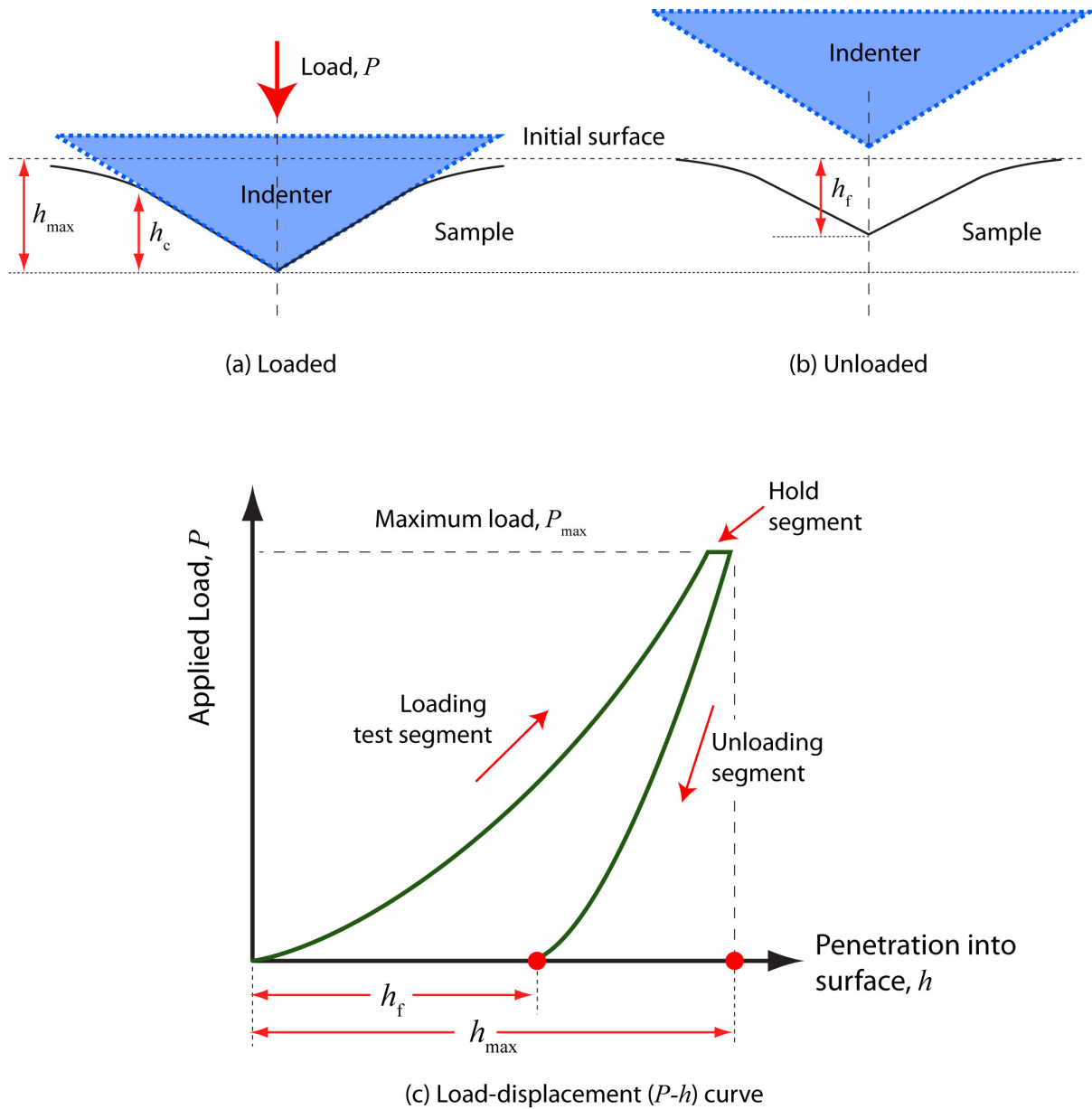


Figure S2: Schematics illustrating the geometry of the (a) loading and (b) unloading test segments using a Berkovich nanoindenter tip (After⁶). The contact depth developed under load, h_c , can be determined from eqn.(4). (c) A typical load-displacement ($P-h$) curve, where h_{\max} denotes the maximum indentation depth (~ 500 nm in this study) and h_f is the depth of the residual indent at 100% unload.

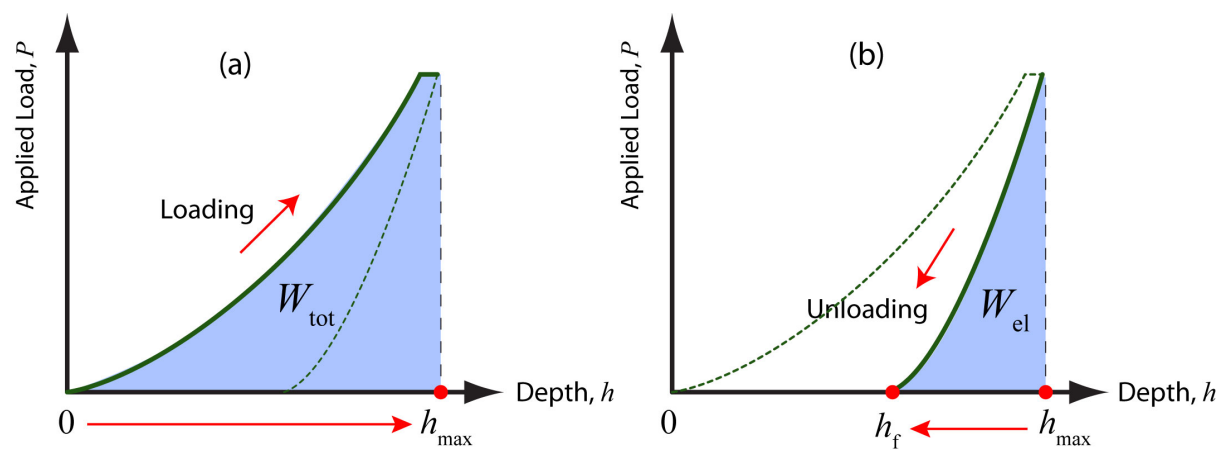


Figure S3: The shaded areas under the load-displacement curves designate (a) the total work done during loading, and (b) the elastic work recovered during unloading.

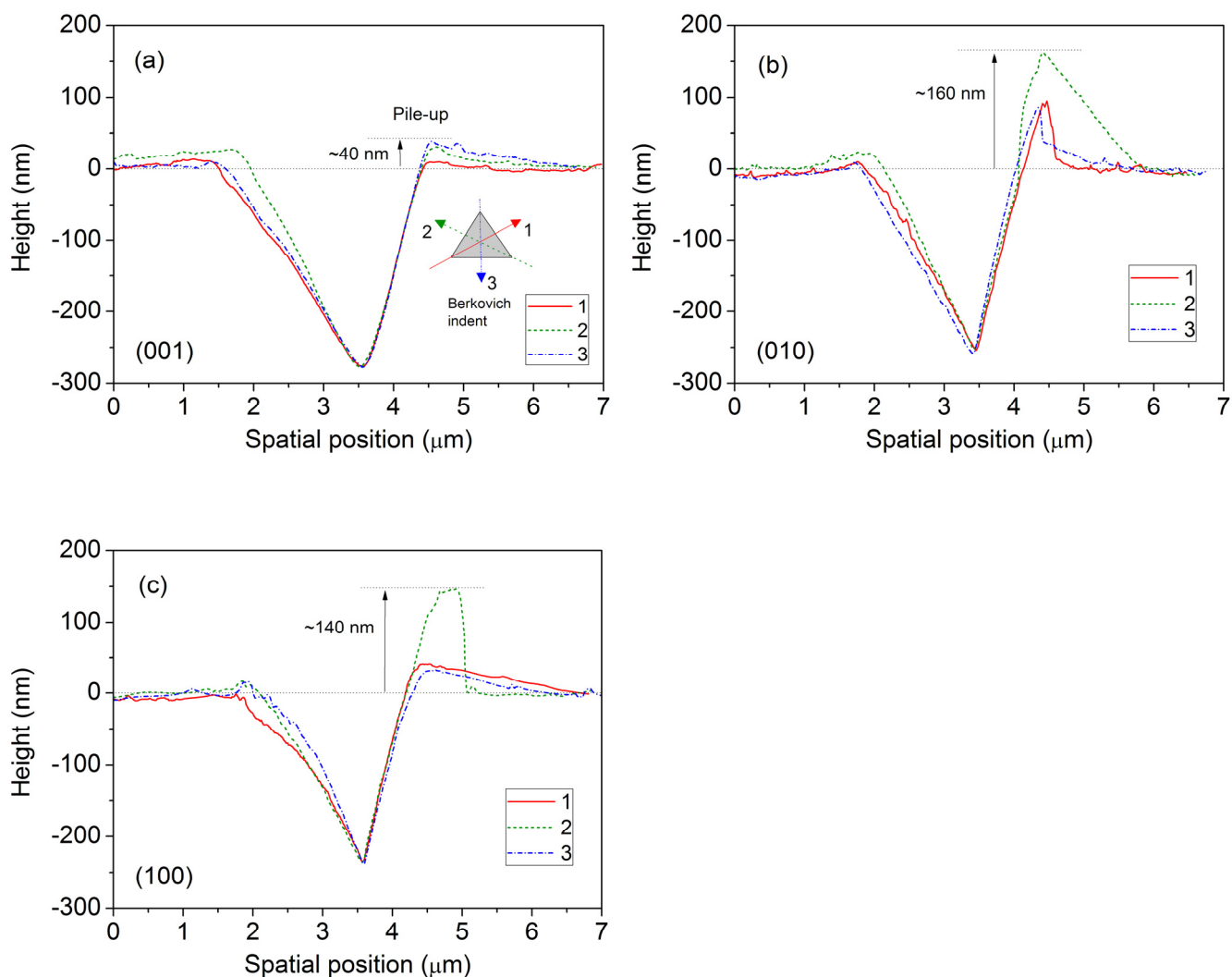


Figure S4: Typical AFM height topography obtained from the residual Berkovich indents made on the (001)-, (010)- and (100)-oriented crystal facets. The cross-sectional profiles correspond to the three designated directions depicted in the inset of (a). It can be seen that the shape of the pile-up developed around the indenter tip is strongly correlated to the orientation of the crystal facet, which also indicates different strain hardening behavior. As expected, the (001)-oriented facet exhibits the least amount of pile-up (~ 40 nm) since it can undergo extensive strain hardening in the plastic regime. On the contrary, the (100)- and (010)-oriented planes that are elastic perfectly plastic tend to show more pile-up, here - ranging from 50 nm to 150 nm. These observations are consistent with the strain-strain curves derived from spherical indentation data (see Figure 3 inset in the Manuscript).

References

- (1) Romero, S.; Mosset, A.; Trombe, J. C. *J. Solid State Chem.* **1996**, *127*, 256-266.
- (2) Sheldrick GM. SADABS - Siemens Area Detector Absorption Correction Program. University of Göttingen, Göttingen, Germany, 1994.
- (3) Sheldrick GM. SHELXTL-PLUS Program for Crystal Structure Solution and Refinement. University of Göttingen, Göttingen, Germany, 1997.
- (4) Oliver, W. C.; Pharr, G. M. *J. Mater. Res.* **2004**, *19*, 3-20.
- (5) Fisher-Cripps, A. C. *Nanoindentation*; 2nd ed.; Springer, New York, 2004.
- (6) Oliver, W. C.; Pharr, G. M. *J. Mater. Res.* **1992**, *7*, 1564-1583.
- (7) Spary, I. J.; Bushby, A. J.; Jennett, N. M. *Philos. Mag.* **2006**, *86*, 5581-5593.
- (8) Field, J. S.; Swain, M. V. *J. Mater. Res.* **1993**, *8*, 297-306.
- (9) Johnson, K. L. *Contact Mechanics*; Cambridge Univ. Press: Cambridge, 1985.